Chinese Journal of Physics 92 (2024) 1267–1274

Contents lists available at ScienceDirect

Chinese Journal of Physics

journal homepage: www.sciencedirect.com/journal/chinese-journal-of-physics

Research Paper

The evolution of dissipative soliton resonance from noise-like pulse via the saturable absorption to reverse saturable absorption transition within covalent organic framework saturable absorbers

Hsuan-Sen Wang [a], Ahmed F.M. EL-Mahdy [b], Shiao-Wei Kuo [b], Wen-Hsuan Kuan [c], Kuei-Huei Lin [c], Gong-Ru Lin [*,d], Chao-Kuei Lee [*,a]

[a] Department of Photonics, National Sun Yat-Sen University, Kaohsiung, 80424, Taiwan
[b] Department of Materials and Optoelectronic Science, National Sun Yat-Sen University, Kaohsiung, 80424, Taiwan
[c] Department of Applied Physics and Chemistry, University of Taipei, Taipei 10048, Taiwan
[d] Graduate Institute of Photonics and Optoelectronics and Department of Electrical Engineering, National Taiwan University, Taipei 10617, Taiwan

ARTICLE INFO

Keywords:
Covalent organic framework
Dissipative soliton resonance
Saturable absorber
Reverse saturable absorption

ABSTRACT

In this study, for the first time, the dynamic evolution from noise-like pulses (NLPs) to dissipative soliton resonance (DSR) in an erbium-doped fiber laser system was observed and investigated by using a porphyrin/pyrene-linked covalent organic framework (COF) saturable absorber. Experimentally, by adjusting the pump power, the laser operation state was observed to be with a transition from NLPs to DSR. In addition, the correlation between the transition from NLPs to DSR and the variation from saturable absorption to reverse saturable absorption (RSA) within the COF material was analyzed, leading to the variation of absorption with increasing pump power playing a key role in this process. The competition mechanism between the spectral filtering effect and RSA was proposed, and the results observed agree quite well with the proposed model. This research not only reveals new features of pulse dynamics in fiber lasers but also highlights the potential of crystalline porous materials in nonlinear optical applications. It provides an important experimental foundation for further exploration of novel two-dimensional materials in the field of ultrafast optics.

1. Introduction

Solitons are typically considered stable, self-contained objects that do not exhibit any chaotic behavior [1]. This is true for solitons in integrable systems but not necessarily for those in dissipative systems. In general, dissipative solitons exist in various physical systems, including binary fluids and all-optical transmission lines. Dissipative solitons are the result of a complex balance between dispersion, nonlinearity, gain, and loss within the fiber laser cavity. In many cases, this intricate equilibrium results in solitons with fixed shapes. In the last few decades, the concept of solitons has also been widely applied in studying the pulse characteristics of ultrafast fiber lasers [2]. Unlike typical solitons generated in fiber lasers, the formation of dissipative solitons requires additional nonlinear losses, described by a term that depends quadratically on intensity [3]. This extra nonlinear loss can be induced through

* Corresponding author.
E-mail addresses: ahmedelmahdy@mail.nsysu.edu.tw (A.F.M. EL-Mahdy), kuosw@faculty.nsysu.edu.tw (S.-W. Kuo), whkuan@utaipei.edu.tw (W.-H. Kuan), khlin@utaipei.edu.tw (K.-H. Lin), grlin@ntu.edu.tw (G.-R. Lin), chuckcklee@yahoo.com (C.-K. Lee).

https://doi.org/10.1016/j.cjph.2024.10.028
Received 9 August 2024; Received in revised form 4 October 2024; Accepted 23 October 2024
Available online 16 November 2024

spectral filtering effects or reverse saturable absorption (RSA) in the cavity. Notably, the dissipative solitons are a special form of ultrashort pulses, all possessing the same profile and energy within the laser cavity. The energy, profile, and chirp of these dissipative solitons are predetermined by the parameters of the governing equations, rather than the initial conditions. These characteristics provide an important platform for studying how to produce stable trains of laser pulses in mode-locked cavities [4].

Among various pulsed fiber lasers, noise-like pulses (NLPs) are a special form of dissipative solitons characterized by containing multiple sub-pulses within the overall pulse envelope [5]. These sub-pulses exhibit random variations in amplitude, duration, and time intervals. Consequently, the corresponding autocorrelation (AC) trace will display a characteristic narrow coherent peak superimposed on a broad, smooth pedestal extending over a long temporal range [6]. Despite their inherent randomness, NLPs have exhibited considerable potential in various applications [7]. For example, the low temporal coherence of NLPs effectively reduces coherent noise, making them highly suitable for applications such as optical coherence tomography and low-coherence interferometry [8]. Furthermore, the broad and smooth spectrum of NLPs helps generate flat supercontinuum sources [9], and their high pulse energy offers wide potential in micromachining and material processing [10]. On the other hand, dissipative soliton resonance (DSR) is another important pulse phenomenon in ultrafast fiber lasers. DSR pulses are characterized by a near-rectangular temporal envelope, with the pulse width increasing while the peak power remains constant as the pump power increases. In the DSR regime, the pulse energy can increase indefinitely with pump power without pulse breakup, as the pulse broadens temporally while maintaining a constant peak power [11]. Compared to NLPs, DSR pulses typically exhibit higher stability. The key differences between DSR pulses and NLPs are evident in their temporal profiles and stability characteristics. DSR pulses have a well-defined, stable rectangular shape, while NLPs consist of sub-pulses with random intensity fluctuations within an overall envelope. DSR pulses are highly stable from pulse to pulse, maintaining their characteristic shape and properties, while NLPs exhibit significant pulse-to-pulse fluctuations.

Saturable absorbers (SAs) are crucial in passively mode-locked fiber lasers. In recent years, two-dimensional (2D) materials such as graphene, transition metal dichalcogenides, and emerging inorganic 2D materials [12–16] have been extensively studied as SAs. Recently, as an emerging branch of 2D materials, crystalline porous materials such as metal-organic frameworks (MOFs) and covalent organic frameworks (COFs) have shown excellent saturable absorption properties and great potential in passively mode-locked fiber lasers [17,18]. COFs are built by linking organic building blocks through dynamic covalent linkages. The robust covalent linkage in COFs endows them with higher stability than many MOFs [19]. As SAs, COFs offer unique advantages due to their tunable structures. Their nonlinear optical properties can be precisely engineered by selecting different organic monomers. Notably, some COFs exhibit a transition from saturable absorption to reverse saturable absorption (RSA) [20], a key feature for achieving the dynamic transition from NLPs to DSR. This research advances our understanding of pulse dynamics in fiber lasers and opens new possibilities for COFs in ultrafast optics. It enables the exploration of complex pulse dynamics at lower intracavity intensities, potentially leading to versatile applications in ultrafast fiber laser systems.

In this work, using a porphyrin/pyrene-linked COF SA, 1.5 μm wavelength region erbium-doped fiber NLPs are investigated and successfully generated. Moreover, on the basis of the rich nonlinear absorption characteristics of COFs, we discovered that upon further increasing the pump power, the laser's operational state transitions from NLPs to DSR. This dynamic change in the laser strongly depends on the peak intensity within the cavity and conforms to theoretical predictions, providing a robust platform for studying the dynamic behaviors of dissipative solitons in fiber lasers.

2. Experimental setup and nonlinear optical response of COF SAs

The novel π-electron-extended porphyrin/pyrene-linked COF (PorPh-PyTACOF) from the new PorPh-4CHO building was prepared by solvothermal method [21]. First, a novel PorPh-PyTA-COF was synthesized solvothermally through the one-pot reaction of PorPh-4CHO, a new building block, and PyTA-4NH_2 in a mixture of *n*-butanol, *o*-dichlorobenzene, and 6M acetic acid (4 mL: 4mL: 0.8 mL) in a 25 mL Schlenk storage tube. The tube was sealed and degassed through three freeze/pump/thaw cycles. The tube was sealed off by flame and heated at 120 °C for 3 days. After cooling to room temperature, the tube was opened, and the precipitate was filtered off and washed two times, each with n-BuOH, THF, and acetone. Then, the solid was dried under a vacuum at 120 °C overnight to obtain a powder. The crystalline PorPh-PyTA-COF had self-assembled to generate non-regular dark and dense spheres with a layered structure and optically translucent features. The average diameter of the spherical features on the PorPh-PyTA-COF is 175 ± 30 nm.

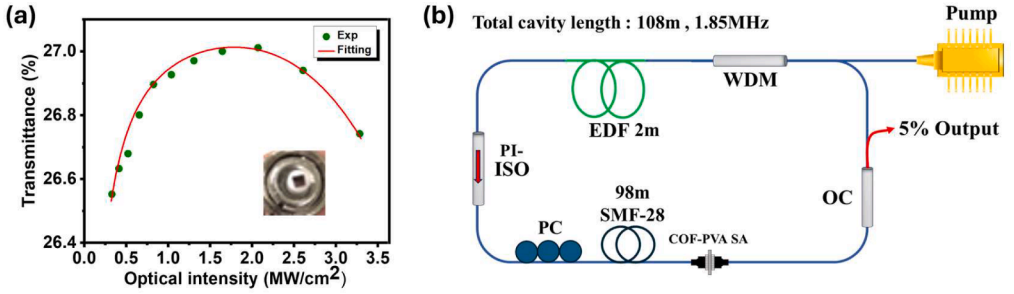

Fig. 1. (a) Experimental nonlinear optical transmittance and corresponding fitting curve. The inset is the surface of the fiber connecter with the COF-PVA film. (b) Experimental setup of the erbium-doped fiber laser with the COF-PVA SA.

The PorPh-PyTA-COF exhibited high crystallinity, a very large Brunauer–Emmett–Teller (BET) surface area (843 $m^2\ g^{-1}$), extreme thermal stability (up to 525 °C), and ultrahigh chemical stability in various organic solvents [22]. After that, PorPh-PyTA-COF powder is embedded into polyvinyl alcohol (PVA) film to fabricate the COF-based SA (COF-PVA SA). The nonlinear absorption characteristics of the COF-PVA SA are recorded using a dual-detector setup [23]. The measurement utilized a homemade nonlinear polarization rotation (NPR) mode-locked erbium-doped fiber laser, which was amplified by an erbium-doped fiber amplifier (EDFA). This laser source operated at a repetition rate of 40 MHz, producing pulses with a duration of 3 ps after the amplifier. The nonlinear absorption characteristics of the COF-PVA SA are depicted in Fig. 1(a), where the SA exhibits both saturable absorption and reverse saturable absorption (RSA) behavior. As the light intensity increases from 0.3 MW cm^{-2} to 1.7 MW cm^{-2}, the increasing transmittance demonstrates saturable absorption behavior. When the optical intensity further increases and exceeds 1.7 MW cm^{-2}, the transmittance decreases, indicating RSA. The RSA behavior can be primarily attributed to the excited-state absorption process. At low intensities, absorption occurs mainly from the ground state to the excited state. At higher intensities, absorption from the excited state to higher-lying states becomes dominant, leading to an increase in overall absorption with increasing intensity [24].

The erbium-doped fiber laser (EDFL) cavity with the COF-PVA SA is depicted in Fig. 1(b). The gain medium is a 2 m-long erbium-doped fiber with an absorption coefficient of 80 dB m^{-1} at 1531 nm. A 976 nm laser diode serves as the pump source. The laser cavity is composed of several components, including a 980/1550 nm wavelength-division multiplexer (WDM), a 95:5 output coupler (OC), a polarization-independent optical isolator (PI-ISO), and a COF-PVA SA positioned between two FC/PC fiber connectors. The end facet of the fiber connector is shown in the inset of Fig. 1(a). To provide sufficient nonlinearity for generating NLPs, an additional 98 m of single-mode fiber is added to the original 10 m of total cavity length, bringing the total length of the laser cavity to approximately 108 m. A portion of the light from the cavity is extracted through the output coupler for characterization and monitoring. An optical spectrum analyzer is used to evaluate the pulse spectrum. Optical signals are converted to electrical signals using a photodetector with an oscilloscope to measure the time-domain waveform of the output pulse trains. Additionally, an RF spectrum analyzer is employed to determine frequency signals. To minimize the impact of environmental factors, the fiber laser system was securely fixed to an optical table to reduce mechanical vibrations. Additionally, air conditioning was maintained throughout the experiment to stabilize the environmental temperature, thus minimizing its influence on the experimental outcomes.

3. Results and discussion

The output power characteristics of the EDFL are shown in Fig. 2(a). After appropriate adjustment of the polarization controller, the laser starts lasing with continuous-wave (CW) operation when the pump power reaches 211 mW. At a pump power of 241 mW, the laser reaches the mode-locking threshold. As depicted in Fig. 2(b), pulse envelope generation begins with a period of 540 ns, matching the cavity length of the resonator. The observed high laser threshold of over 200 mW for EDFL with COF-PVA SA laser can be primarily attributed to the relatively high non-saturable absorption loss of the COF-based saturable absorber. This property results in increased overall cavity losses, necessitating higher pump powers to overcome these losses and achieve the required gain for lasing and mode-locking. From 241 mW to 331 mW, it can be observed that the pulse envelopes do not have a significantly ordered structure. As the pump power gradually increases within this range, the pulse envelope expands correspondingly. However, a significant change in pulse behavior is observed at higher pump powers. We note that the pulse envelopes transition into a single, complete pulse with markedly increased peak power when the pump power is raised above 361 mW. To confirm the transition in the laser state, we measured the spectral signals using an RF spectrum analyzer.

As shown in Fig. 3(a), at a pump power of 211 mW, the output is in a CW state, and consequently, there is no signal on the RF spectrum. When the pump power reaches 241 mW, pulses begin to appear, along with a signal at a fundamental frequency of 1.85 MHz. This observation is consistent with the initial transition to the mode-locking state described earlier. As the power increases, the number of harmonic frequencies in the signal gradually increases. Below 331 mW, there are considerable intensity fluctuations at higher harmonics. When the pump power is raised above 361 mW, the spectrum exhibits a signal with amplitude modulation similar to a sinc function. This sinc-like pattern is characterized by a central peak at the fundamental frequency, followed by symmetrical side lobes that decrease in amplitude as they move away from the center. This pattern is typical of pulsed laser output in the frequency domain.

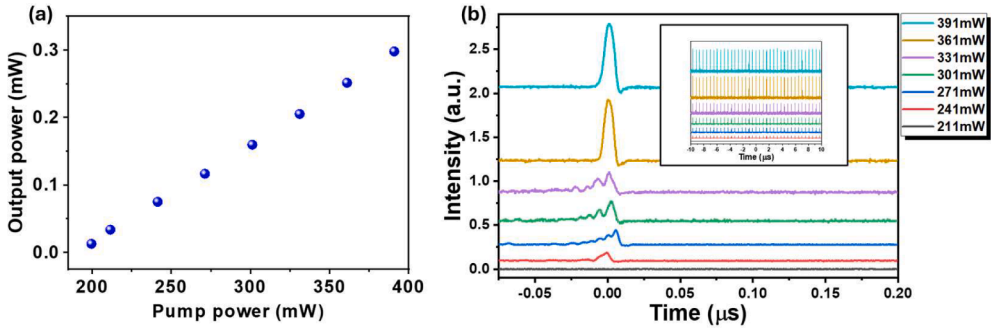

Fig. 2. The character of the erbium-doped fiber laser with the COF-PVA SA: (a) output power and (b) pulse envelope profile (inset: pulse trains vs. pump power).

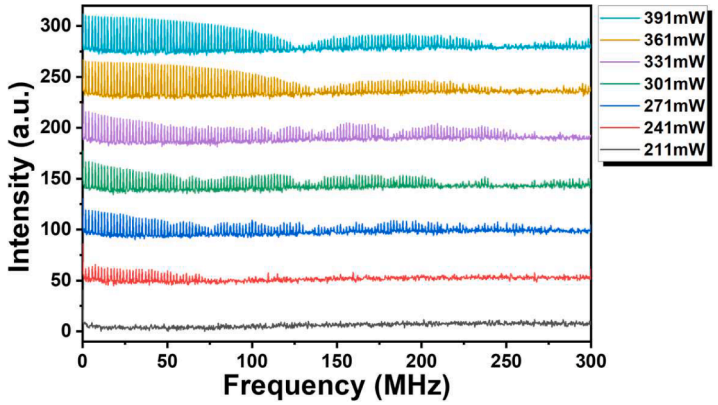

Fig. 3. The RF spectrum of the erbium-doped fiber laser with the COF-PVA SA vs. pump power.

The zeros of this sinc-like function correspond to the nulls between the harmonic peaks, with the first zero occurring at a lower frequency, indicating a wider pulse envelope in the time domain. This distinctive spectral pattern signifies a stable extension of harmonic frequencies, which is characteristic of a pulse train exhibiting a near-rectangular temporal envelope and a broadening pulse width.

To further convince and identify the state of pulses, the autocorrelation (AC) trace was therefore taken here; see Fig. 4. Noise-like pulses (NLPs) typically exhibit distinctive features in their AC traces. These include a narrow coherent peak superimposed on a broad, smooth pedestal extending over a longer temporal range [6]. This extended pedestal indicates internal intensity fluctuations within the pulse envelope, which are characteristic of NLPs. At lower pump powers of 271 mW and 331 mW, the observed AC traces display typical NLP features. The traces show a narrow coherent peak superimposed on a broad, smooth pedestal extending beyond the 40 ps measurement window, consistent with expected NLP behavior. In addition, the peak-to-pedestal ratio in the AC trace has been recognized as a key indicator of the pulse's noise-like nature, suggesting that most of the pulse amplitude comprises noise with little ordered structure. At the lower pump power of 271 mW, the coherent peak-to-pedestal level ratio is approximately 2:1. This low ratio aligns with NLP characteristics described in the literature [6], indicating a pulse structure dominated by noise-like fluctuations with low coherence. As pump power increases to 331 mW, this ratio rises to about 4:1, suggesting a slight increase in pulse coherence while maintaining overall NLP characteristics. After that, significant changes in the AC traces are observed as pump power exceeds 361 mW. The pedestal level rises noticeably, and a central spike accompanied by edge dips appears in the middle of the pedestal. These changes in the AC trace indicate a substantial alteration in pulse structure. Such AC trace features closely match the predicted temporal characteristics of DSR pulses under anomalous dispersion conditions in literature [25]. Specifically, the broad and elevated pedestal corresponds to the square-wave body of the DSR pulse. Under anomalous dispersion, frequency components from the pulse edges move toward the pulse center. When chirped wave packets from the left and right pulse edges meet at the center, they interfere, producing an intensity peak at the pulse center with accompanying edge dips. This comprehensive analysis of AC traces provides clear evidence of the transition from NLP to DSR regimes as pump power increases. One should note that these results and analyses also echo the observation and discussion done with the time domain and RF spectrum, indicating that time domain behavior can be a reliable reference for judging NLPs and DSR.

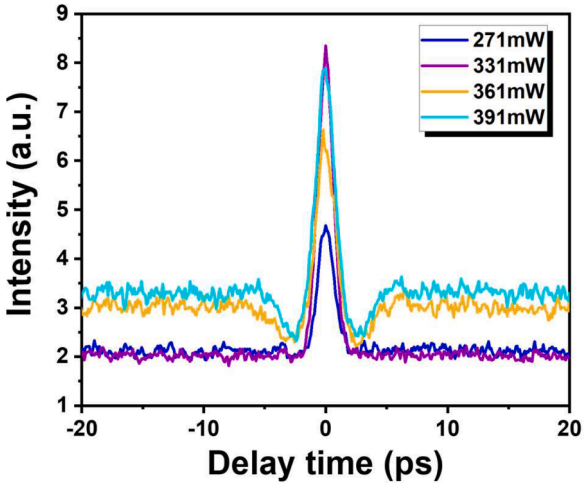

Fig. 4. The autocorrelation trace of the laser output vs. pump power.

Furthermore, we analyze the long-term (100 ms) variation of fundamental resonance frequency within the RF spectrum in amplitude and frequency. Fig. 5(a) displays the RF spectra at the fundamental resonance frequency (approximately 1.85 MHz) under different pump powers. A significant increase in spectral amplitude is observed as the pump power increases from 241 mW to 391 mW. The upper parts of Fig. 5(b) and (c) show the temporal variations of amplitude and frequency of the fundamental resonance frequency at different pump powers. To quantitatively assess the degree of amplitude and frequency variations, the coefficient of variation (CV) for amplitude and the mean absolute deviation (MAD) for frequency were calculated. The coefficient of variation is defined as:

$$\mathrm{CV} = \sigma/\mu \tag{1}$$

where σ is the standard deviation, and μ is the mean value. This normalized estimation allows for the comparison of the temporal fluctuation of amplitude. In addition, to evaluate the variation of the resonance frequency, the mean absolute deviation is defined and calculated as:

$$\mathrm{MAD} = \sum \frac{|x-\mu|}{N} \tag{2}$$

where x represents individual data points, μ is the mean of the dataset, and N is the total number of data points. The CV and MAD are accordingly estimated and plotted; see the lower parts of Fig. 5 (b) and (c). The results clearly demonstrate that both amplitude and resonance frequency instabilities significantly decrease with pump power. Besides, compared to the DSR state (pump power 361 and 391 mW), the larger fluctuations in both amplitude and resonance frequency are observed under the NLP state (pump power 241 to 331 mW). This analysis not only provides a complete picture of pulse behavior but also clearly reflects the nature of the NLP, which exhibits chaotic and irregular motions within pulse envelopes.

After confirming the transition from NLPs to the DSR regime through AC trace analysis, we further investigated the characteristic pulse-broadening behavior of DSR. A typical phenomenon in DSR is the pulse width broadening as the pump power is enlarged [26]. The corresponding DSR pulse profiles are shown in Fig. 6. As the pump power increases from 361 mW to 391 mW, we observe a broadening of the pulse width from 6.4 ns to 6.9 ns. This clearly agrees well with the nature of the pulse width broadening as the pump power is enlarged under DSR operation.

Additionally, the optical spectrum of the laser output under various pump powers is characterized. Fig. 7(a) shows the optical spectra for pump powers ranging from 211 to 301 mW. When the pump power is 211 mW, the laser exhibits CW lasing with a central wavelength of 1570 nm. At 241 mW, the corresponding spectrum markedly broadens, attributed to the self-phase modulation (SPM), while dispersive wave signals appear at 1567 nm and 1572.7 nm on both sides of the central wavelength [27]. As the pump power is further increased, the peak intensity at the central wavelength of 1570 nm is limited, and the tendency of spectral broadening is more gradual. Simultaneously, the progressively intensified signals of the dispersive waves were recorded. This phenomenon indicates that the intensity at the central wavelength is limited while the dispersive waves are enhanced. Fig. 7(b) displays the spectra for pump powers from 301 to 391 mW. At the earlier stage, from 301 to 331 mW, a slightly broadened spectrum with distinct sharp peaks was

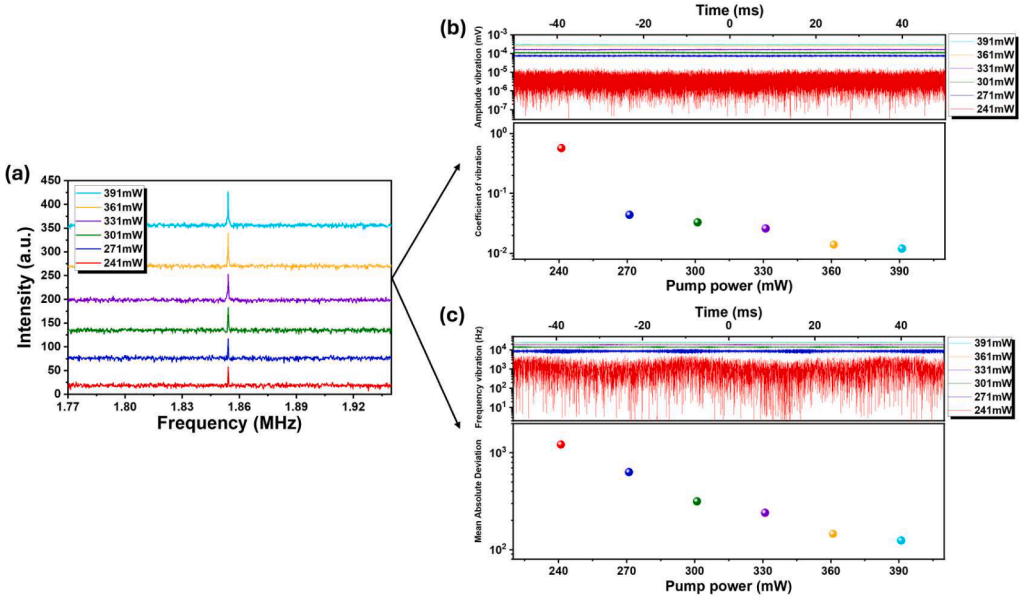

Fig. 5. Characteristics of the erbium-doped fiber laser with COF-PVA SA. (a) RF spectrum for the fundamental resonance frequency at various pump powers (b) and (c) Variations in the amplitude and frequency of the signal, respectively, monitored over a 100 ms period at different pump powers. The upper panels show the temporal fluctuations, while the lower panels display the coefficient of variation for amplitude and the mean absolute deviation for resonance frequency as functions of pump power.

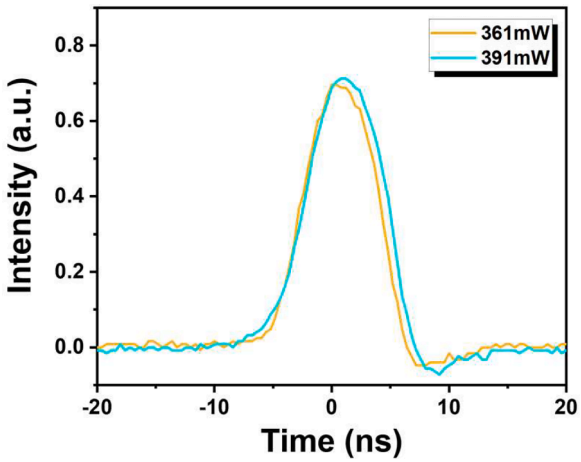

Fig. 6. Temporal profiles of single pulses at pump powers of 361 mW and 391 mW.

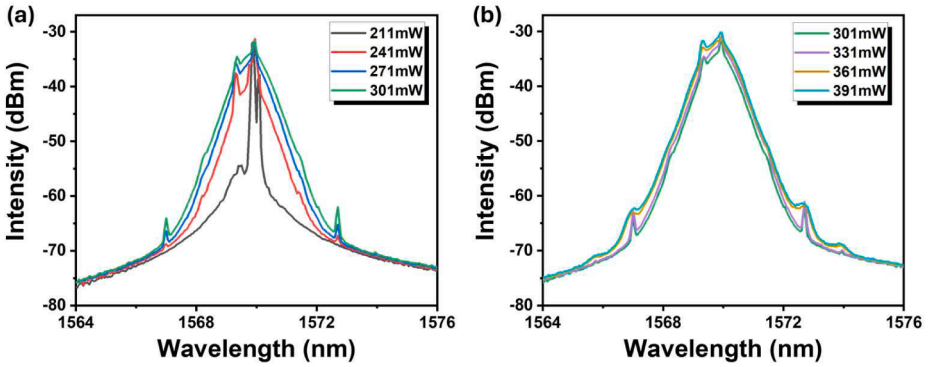

Fig. 7. The erbium-doped fiber laser with the COF-PVA SA: optical spectrum vs. pump power.

characterized on both edges. As the pump power further increases from 331 to 361 mW, the sharp peaks on both sides become blurred. When the pump power is increased from 361 to 391 mW, the spectrum exhibits almost no broadening. This lack of spectral broadening indicates a clamping of the SPM effect. Concurrently, the signals of the dispersive waves on both sides of the central wavelength are not continuously amplified.

From the experimental results discussed above, a transition from NLPs to DSR in an EDFL system utilizing a ProPh-PyTA-COF SA is observed. To further demonstrate the reliability of the experimental results, we conducted stability tests of the pump power. Two representative power levels for long-term stability testing, 241 mW (corresponding to the NLP state) and 361 mW (corresponding to

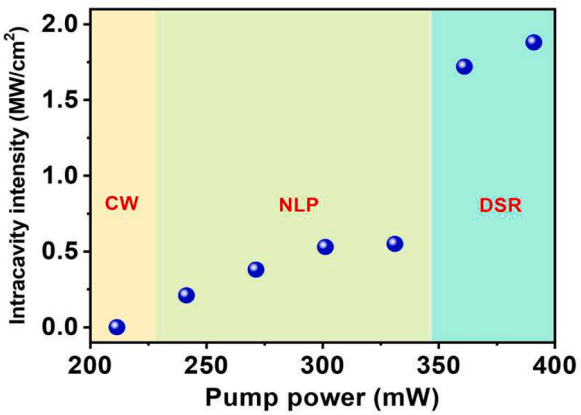

Fig. 8. Intracavity intensity vs. pump power for various laser operation states.

the DSR state), are selected. We continuously monitored these power levels for 1 h each. The results showed that throughout the entire monitoring period, pump power fluctuations remained within ±0.35 %, confirming the reliability of the experimental results. Furthermore, this study demonstrated the excellent long-term stability of the fiber laser system based on the COF saturable absorber. Over a six-month experimental period, the laser performed reproducible results throughout, revealing the exceptional durability of the COF material in practical applications and providing strong evidence for its viability in ultrafast optical systems.

According to the research by Du et al., the transition from NLPs to DSR involves the competition between the spectral filtering effect and RSA effect induced by the SA material [28]. The spectral filtering effect plays the main role while pumping with low power since the RSA effect is weak. The interaction between dispersive waves and solitons will lead to NLP generation. In contrast to the low pump power, the RSA effect dominates at higher pump powers. The spectral broadening will be limited, and DSR operation will be promoted. Fig. 8 plotted intracavity peak intensity versus pump power. The laser operates in a CW state at a pump power of 211 mW, indicating nearly zero peak intensity inside the cavity. The laser changes to NLPs while pump power increases to 241 mW, see Fig. 2(b). From the AC traces and RF spectrum, the lasers operate under the state of NLP for a pump power of 241 mW to 331 mW. The peak intensity inside the cavity can be accordingly calculated to be 0.2 to 0.55 mW cm^{-2}. When the pump power exceeds 361 mW, the laser operates to become DSR. The peak intensity of 1.72 and 1.88 mW cm^{-2} can also be estimated for the pump power of 361 and 391 mW, respectively. One should note that the NLPs and DSR regions are correlated with the saturable absorption and RSA, as observed in Fig. 1(a). Apparently, our results agree quite well with the theoretical prediction. The evolution mechanism from NLPs to DSR can be attributed to the pump power range: from 241 mW to 331 mW, weaker RSA, and stronger spectral filtering favor NLP generation. When the pump power increases to 361 mW, the RSA effect becomes dominant, driving the transition to DSR.

Typically, the transition from saturable absorption to RSA requires a considerable change in peak intensity, which is challenging to achieve. Fortunately, with the aid of the complex band structure of COF-based SAs, the fruitful nonlinear absorption behavior makes it possible [29]. Within a specific intensity range, a narrow transition from saturable absorption to RSA occurs over an interval of approximately 1 mW cm^{-2}. This allows us to observe this transition in actual fiber laser systems and potentially leads to changes in the pulse behavior within the cavity. Besides, this work not only advances our understanding of pulse dynamics in fiber lasers but also opens new avenues for the application of COFs in the field of ultrafast optics. Moreover, this work also paves the way for investigating complex pulse dynamics at relatively low intracavity intensities, leveraging the exceptional properties of COFs and marking a pivotal advancement in the development of next-generation ultrafast laser systems. Further studies on the nonlinear optical properties and applications of various dynamics within fiber lasers using different 2D materials are still ongoing. The results will be helpful for understanding fiber laser technology in detail and are expected to open new prospects for the application of novel 2D materials in ultrafast optics.

4. Conclusion

This research reports the first experimental observation of NLPs and their transition to DSR in an erbium-doped fiber laser system utilizing a COF-based SA. The experimental results of the RF spectrum and autocorrelation trace show that by adjusting the pump power, the laser operational state can be switched from NLPs to DSR, and this transition is closely related to the peak intensity within the cavity. Notably, the transition from saturable absorption to RSA occurs at an intensity of approximately 1.7 mW cm^{-2}. This low transition threshold plays a crucial role in facilitating the observation of the NLPs to DSR transition within the practical operating range of the fiber laser system. Specifically, when the pump power reaches a certain level, the RSA characteristics of the COF lead to the switching of NLP to DSR state. The competition mechanism between the spectral filtering effect and RSA was proposed, and the results observed agree quite well with the proposed model. This research demonstrates that crystalline porous materials such as COFs have considerable potential in nonlinear optics, especially in generating ultrashort pulses. Additionally, our findings provide a robust experimental foundation for further research and application of novel 2D materials in ultrafast optics.

CRediT authorship contribution statement

Hsuan-Sen Wang: Writing – original draft, Formal analysis, Data curation. **Ahmed F.M. EL-Mahdy:** Resources. **Shiao-Wei Kuo:** Resources. **Wen-Hsuan Kuan:** Validation. **Kuei-Huei Lin:** Writing – review & editing, Validation. **Gong-Ru Lin:** Validation, Resources. **Chao-Kuei Lee:** Writing – review & editing, Conceptualization.

Declaration of interests

The authors declare that they have no known competing financial interests or personal relationships that could have appeared to influence the work reported in this paper.

Acknowledgment

This work is supported by the National Science and Technology Council, Taiwan (NSTC) under Contract No. NSTC-112-2112-M-110-016 and NSTC 113-2112-M-110-017.

References

[1] A.C. Newell, Solitons in mathematics and physics, Society for Industrial and applied Mathematics, 1985.
[2] G.P. Agrawal, Chapter 5 - optical solitons, in: G. Agrawal (Ed.), Nonlinear Fiber Optics (Fifth Edition), Academic Press, 2013, pp. 129–191, https://doi.org/10.1016/B978-0-12-397023-7.00005-X.
[3] A. Komarov, F. Amrani, A. Dmitriev, K. Komarov, F. Sanchez, Competition and coexistence of ultrashort pulses in passive mode-locked lasers under dissipative-soliton-resonance conditions, Phys. Rev. A: Atom. Mol. Opt. Phys. 87 (2) (2013), https://doi.org/10.1103/physreva.87.023838.
[4] P. Grelu, N. Akhmediev, Dissipative solitons for mode-locked lasers, Nat. Photonics. 6 (2) (2012) 84–92, https://doi.org/10.1038/nphoton.2011.345.
[5] P. Grelu, Solitary waves in ultrafast fiber lasers: From solitons to dissipative solitons, Opt. Commun. 552 (2024), https://doi.org/10.1016/j.optcom.2023.130035.
[6] M. Horowitz, Y. Barad, Y. Silberberg, Noiselike pulses with a broadband spectrum generated from an erbium-doped fiber laser, Opt. Lett. 22 (11) (1997) 799, https://doi.org/10.1364/ol.22.000799.
[7] N. Kanagaraj, Z. Wang, A. Coillet, P. Tchofo-Dinda, P. Grelu, Buildup of noise-like pulses in ultrafast fiber lasers, in: Paper presented at the 2019 Conference on Lasers and Electro-Optics Europe & European Quantum Electronics Conference (CLEO/Europe-EQEC), Munich, Germany, 2019.
[8] C.-L. Pan, A. Zaytse, Y.-J. You, C.-H. Li, Fiber-laser-generated noise-like pulses and their applications, InTech (2016), https://doi.org/10.5772/61856.
[9] M. Wang, H. Wu, D. Ouyang, M. Liu, Y. Chen, J. Zhao, X. Liu, S. Ruan, High power noise-like pulse at 2 μm and its applications in mid-IR Raman light and flat supercontinuum, Infrared. Phys. Technol. 131 (2023) 104635, https://doi.org/10.1016/j.infrared.2023.104635.
[10] J. Dutta Majumdar, I Manna, Laser material processing, Int. Mater. Rev. 56 (5–6) (2011) 341–388, https://doi.org/10.1179/1743280411Y.0000000003.
[11] A. Komarov, F. Amrani, A. Dmitriev, K. Komarov, F. Sanchez, Competition and coexistence of ultrashort pulses in passive mode-locked lasers under dissipative-soliton-resonance conditions, Phys. Rev. A 87 (2) (2013), https://doi.org/10.1103/physreva.87.023838.
[12] S. Liu, F. Yan, Y. Li, L. Zhang, Z. Bai, H. Zhou, Y. Hou, Noise-like pulse generation from a thulium-doped fiber laser using nonlinear polarization rotation with different net anomalous dispersion, Photonics. Res. 4 (6) (2016) 318, https://doi.org/10.1364/prj.4.000318.
[13] O. Pottiez, R. Grajales-Coutiño, B. Ibarra-Escamilla, E.A. Kuzin, J.C. Hernández-García, Adjustable noiselike pulses from a figure-eight fiber laser, Appl. Opt. 50 (25) (2011) E24, https://doi.org/10.1364/ao.50.000e24.
[14] Z. Wang, Z. Wang, Y. Liu, R. He, S. Han, G. Wang, G. Yang, X. Wang, Noise-like pulses generated from a passively mode-locked fiber laser with a WS_2 saturable absorber on microfiber, Laser. Phys. Lett. 15 (8) (2018) 085103, https://doi.org/10.1088/1612-202x/aac551.
[15] J. Gao, Y. Zhou, Y. Liu, X. Han, Q. Guo, Z. Lu, L. Guo, X. Shang, W. Yang, K. Niu, N. Ming, Z. Wang, H. Zhang, S. Jiang, Noise-like mode-locked Yb-doped fiber laser in a linear cavity based on SnS2 nanosheets as a saturable absorber, Appl. Opt. 58 (22) (2019) 6007, https://doi.org/10.1364/ao.58.006007.
[16] P. Tang, M. Luo, T. Zhao, Y. Mao, Generation of noise-like pulses and soliton rains in a graphene mode-locked erbium-doped fiber ring laser, Front. Inform. Technol. Electron. Eng. 22 (3) (2021) 303–311, https://doi.org/10.1631/fitee.2000372.
[17] X. Jiang, L. Zhang, S. Liu, Y. Zhang, Z. He, W. Li, F. Zhang, Y. Shi, W. Lü, Y. Li, Q. Wen, J. Li, J. Feng, S. Ruan, Y.-J. Zeng, X. Zhu, Y. Lu, H. Zhang, Ultrathin metal-organic framework: an emerging broadband nonlinear optical material for ultrafast photonics, Adv. Opt. Mater. 6 (16) (2018) 1800561, https://doi.org/10.1002/adom.201800561.
[18] H.-S. Wang, A.F.M. EL-Mahdy, S.-W. Kuo, G.-R. Lin, C.-K. Lee, Polarization-dependent covalent organic framework saturable absorber and application of femtosecond fiber laser therein, Chin. J. Phys. (2023), https://doi.org/10.1016/j.cjph.2023.10.040.
[19] Y. Song, Q. Sun, B. Aguila, S. Ma, Opportunities of covalent organic frameworks for advanced applications, Adv. Sci. 6 (2) (2018) 1801410, https://doi.org/10.1002/advs.201801410.
[20] S. Nath, A. Puthukkudi, J. Mohapatra, B.P. Biswal, Covalent organic frameworks as emerging nonlinear optical materials, Angewandte Chemie-Int. Edition 62 (18) (2023), https://doi.org/10.1002/anie.202218974.
[21] H.R. Abuzeid, A.F.M. EL-Mahdy, S.-W. Kuo, Covalent organic frameworks: design principles, synthetic strategies, and diverse applications, Giant 6 (2021) 100054, https://doi.org/10.1016/j.giant.2021.100054.
[22] K.-Y. Chen, H.-S. Wang, S.-P. Su, S.-W. Kuo, C.-K. Lee, A.F.M. EL-Mahdy, Π-electron-extended porphyrin-linked covalent organic framework for a q-switched all-solid-state laser, Adv. Photonics. Res. (2022) 2200145, https://doi.org/10.1002/adpr.202200145.
[23] G. Jiang, L. Miao, J. Yi, B. Huang, W. Peng, Y. Zou, H. Huang, W. Hu, C. Zhao, S. Wen, Ultrafast pulse generation from erbium-doped fiber laser modulated by hybrid organic–inorganic halide perovskites, Appl. Phys. Lett. 110 (16) (2017) 161111, https://doi.org/10.1063/1.4981897.
[24] B.P. Biswal, S. Valligatla, M. Wang, T. Banerjee, N.A. Saad, B.M.K. Mariserla, N. Chandrasekhar, D. Becker, M. Addicoat, I. Senkovska, R. Berger, D.N. Rao, S. Kaskel, X. Feng, Nonlinear optical switching in regioregular porphyrin covalent organic frameworks, Angewandte Chemie 131 (21) (2019) 6970–6974, https://doi.org/10.1002/ange.201814412.
[25] A. Komarov, A. Dmitriev, K. Komarov, D. Meshcheriakov, F. Sanchez, Spectral-doublet rectangular pulses in passive mode-locked fiber lasers with anomalous dispersion, Phys. Rev. A 94 (4) (2016), https://doi.org/10.1103/physreva.94.043827.
[26] J. Lee, J. Koo, J.H. Lee, A pulse-width-tunable, mode-locked fiber laser based on dissipative soliton resonance using a bulk-structured Bi2Te3topological insulator, Opt. Eng. 55 (8) (2016) 081309, https://doi.org/10.1117/1.oe.55.8.081309.
[27] M.L. Dennis, I.N. Duling, Experimental study of sideband generation in femtosecond fiber lasers, IEEe J. Quantum. Electron. 30 (6) (1994) 1469–1477, https://doi.org/10.1109/3.299472.
[28] W. Du, H. Li, J. Li, P. Wang, S. Zhang, Y. Liu, Mechanism of dissipative-soliton-resonance generation in fiber laser mode-locked by real saturable absorber, Opt. Express. 26 (16) (2018) 21314, https://doi.org/10.1364/oe.26.021314.
[29] R. Shi, X. Han, J. Xu, X. Bu, Crystalline porous materials for nonlinear optics, Small. 17 (22) (2021) 2006416, https://doi.org/10.1002/smll.202006416.